

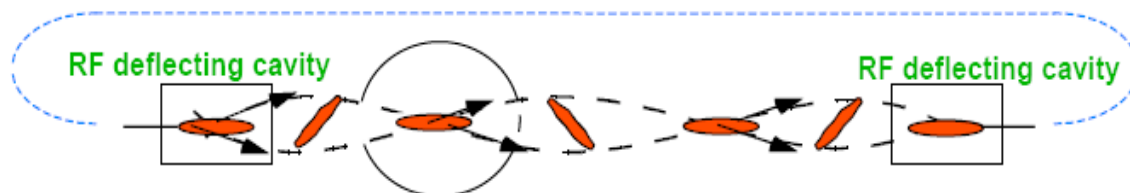
# **Simulation of a Diamond Tilt Monitor for the APS Short Pulse X-ray Source**

Shihao Tian, Hampden-Sydney College  
Supervisor: Bingxin Yang, Argonne National Laboratory  
2011.8.13

## 0. Abstract

The short-pulse x-Ray (SPX) is generated by using RF deflecting cavities. In APS sector 5, a transverse-deflecting RF cavity is used to impose a correlation between the longitudinal position of a particle within the bunch and the vertical momentum; while in sector 7, the second cavity is placed at a vertical betatron phase advance of  $n\pi$

downstream of the first cavity, so as to cancel the correlation. In sector 6, a bend magnet is used to emit photons, which has a strong correlation among time and vertical slope. An x-ray bunch tilt monitor was recently proposed to be based on x-ray beam arrive time (BAT) monitor arrays, and it is used to detect the x-ray phase difference in sector 6. It appears that the physics requirements for the tilt monitor can be realized with current signal processing hardware.



## 1. Device Configuration

In the Advanced Photon Source Upgrade Conceptual Design Report (APS-U CDR), we proposed an x-ray tilt monitor based on x-ray bunch arrival time (XBAT) detector arrays [1]. Recently, we proposed a diamond-on-copper geometry, shown in Figure 1-1, which should handle the x-ray power effectively:

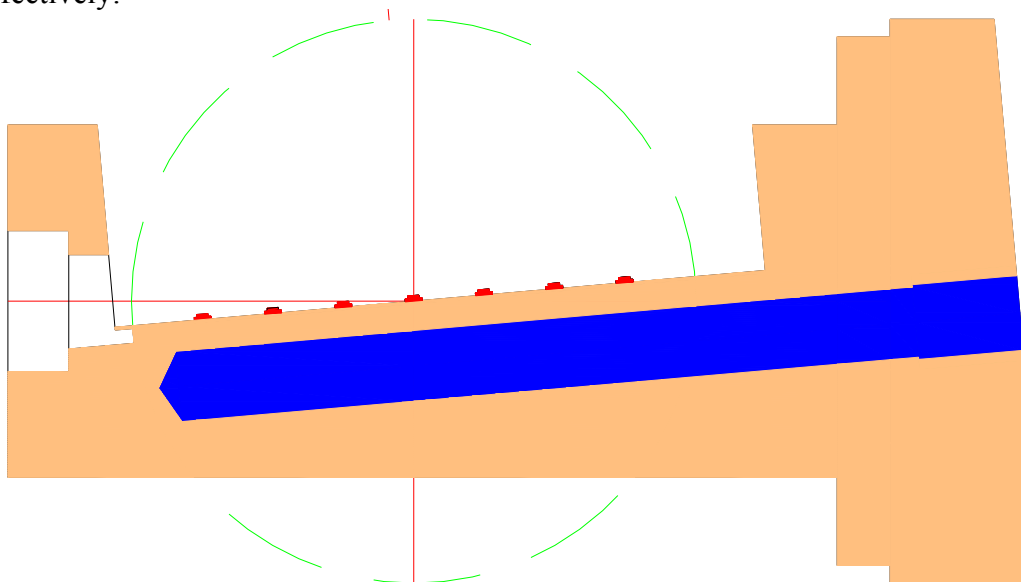


Figure 1-1: An APS bend magnet (BM) tilt monitor.

1. X-ray beam enters the graph from the left and strikes the beam dump in a approximately 10-degree grazing incidence angle. The copper (shown in orange) beam dump has a water-cooling channel (blue) under the surface to carry away the beam-generated heat.
2. The diamond detectors (red) are soldered on the surface for high-efficiency thermal transfer. These detectors operate as solid-state ion-chambers. A high-voltage of 500 – 1000 V is applied across the diamond wafer to obtain maximum transport speed of radiation-induced electrons and holes.
3. Matching networks are etched on the alumina circuit board connecting the diamond detectors to the electric feedthroughs transmitting the signals out of the vacuum chamber.
4. In the processing circuit, the signals will pass through bandpass filters and be compared with a standard timing signal using an S-band phase detector.

The geometry of a single detector is illustrated in Figure 1-2. A 0.5-mm thick (high-quality) diamond detector is used to generate the signal from the x-ray beam. A high-voltage is applied across the diamond to assist the transport of charges. Another 0.5-mm thick diamond circuit board is used to separate the copper beam dump from the diamond detector. Both diamond measure  $1 \times 2.5 \times 0.5 \text{ mm}^3$ .

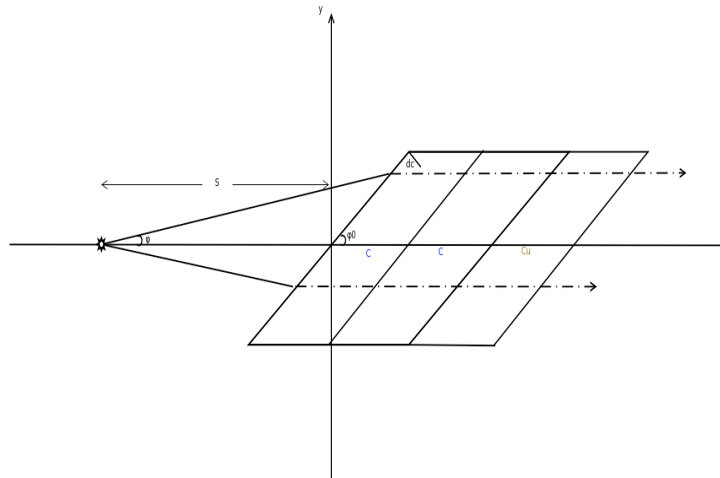


Figure 1-2: Single detector geometry

If the wave front of the incoming x-ray beam is vertical (without chirp), the detectors will generate signals with a series of fixed delays given by the geometry. If however, the x-ray beam bunch is tilted, with x-ray photons above the orbit planes travelling ahead of the bunch center, the top detectors will receive x-ray pulse first and generate signal pulse first, and the bottom detectors will generate later pulses. These systematic deviations give us a measure of the x-ray bunch tilt.

## 2. Simulation of direct signals

To calculate the spatial distribution of the APS bend magnet radiation, we use the programs *ws* written by Roger Dejus [1], which is usually distributed with the XOP program suite [3]. Its output will be converted into SDDS format [4,5] so the SDDS tools developed may be used to calculate the detector responses to the x-ray beam. Tcl and Bourne-shell (sh) scripts are to be used to automate the calculations.

## 2.1 Simulation of bend magnet source

The source calculation is setup as a pinhole-scan experiment. Table 2-1 lists the source and pinhole parameters used for the calculation:

1. We calculate the x-ray spectrum, from 1 to 100 keV, passing through a 1 mm (H)  $\times$  40  $\mu$ m (V) pinhole at 10-mm from the source using the program *ws*. When the pinhole is scanned vertically in 40- $\mu$ m-steps from 6 mm below the orbit plan to +6 mm above the plane, we obtain a collection of 301 beamlets. Each beamlet has its own photon spectrum, and the entire collection of beamlets represents all photons within the 1 – 100 keV energy range through the horizontal aperture of 1 mm at 10 m from the source. Each spectrum is stored as a page in the SDDS file representing the source photon flux (bmFlux0.sdds).
2. Next, we pass each spectrum through a 4-mm beryllium filter, which represents the x-ray window between the storage-ring/front-end vacuum (UHV) and the detector chamber vacuum (HV). This file represents the x-ray photon flux at the detector front surface (bmBeWinFlux.sdds).

Table 2-1: Parameters used for bend magnet spectrum simulation

Parameter	Value	Units
Electron beam energy	7.0	GeV
Electron beam current	1.0	mA
Bend magnet field	0.599	T
Pinhole location (z)	10.0	m
Pinhole width	1.0	mm
Pinhole height	0.04	mm

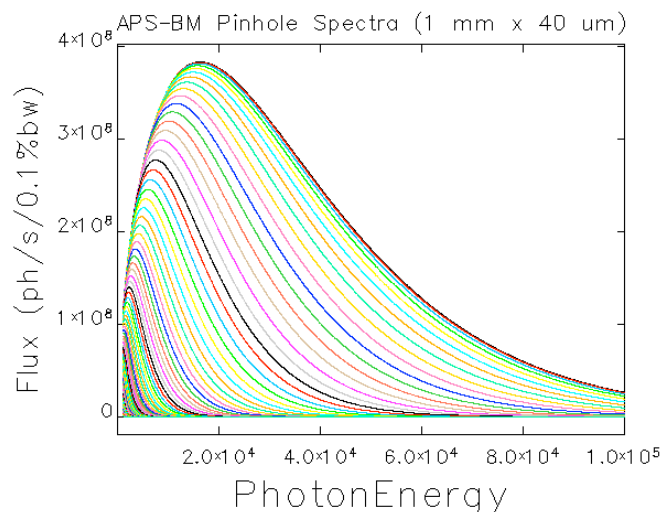


Figure 2-1: The x-ray source spectra viewed through scanning pinholes.

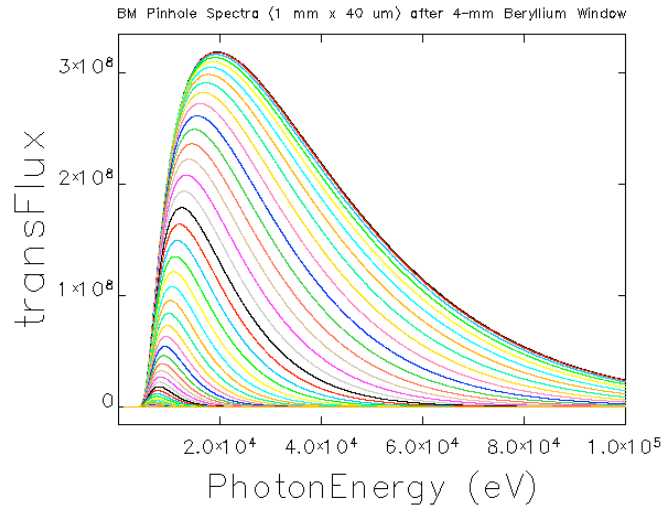


Figure 2-2: The beamlet x-ray spectra after transmitting a 4-mm beryllium window.

Figure 2-1 shows the source flux from the pinholes located 10-m from the source. Figure 2-2 shows the x-ray spectra of these beamlets after passing through a 4-mm beryllium window. Note that the x-ray flux is severely reduced by the beryllium window below 4 keV. If we integrate each spectrum to get the total energy through the pinhole, we may plot the x-ray power as a function of the vertical position of the pinhole, as in Figure 2-3. From the integration of beam power versus the distance to y-axis, we found the total initial beam power is about 80 mW and the total beam power through the beryllium filter is 57 mW, which suggests the that the absorption of the filter is 29%.

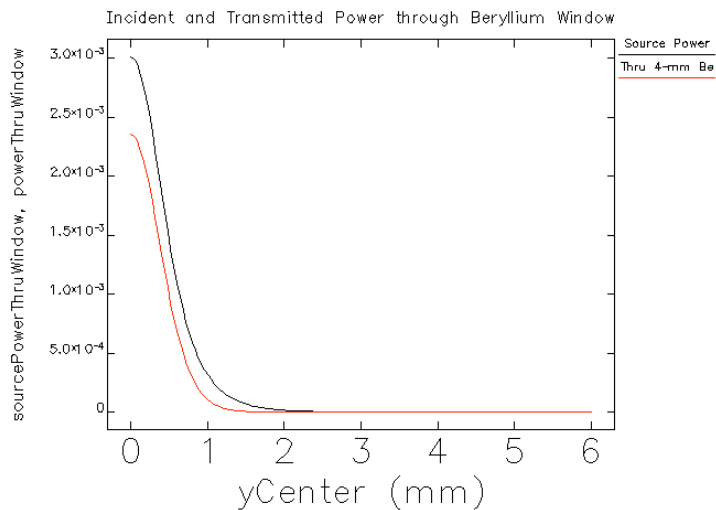


Figure 2-3: The spectral-integrated power as a function of the pinhole's vertical position showing nearly 29% power absorption by the window.

## 2.2 Simulation of primary x-ray absorption and generation of charges in the detector volume

After the beryllium filter, the beam goes through the diamond layer of the detector. In order to calculate the spatial distribution of the absorbed x-ray energy in the diamond detector, we divide the entire detector into several grids, and calculate the absorption of each grid independently. We used the following formula to calculate the absorption of each grid,

$$f_{abs} = I_{(\omega,\varphi)} (1 - e^{-\mu_c \Delta w / \sin \varphi_0})$$

in which  $I(\omega,\varphi)$  is the intensity of the beam,  $\omega$  is the beam frequency,  $\varphi$  is the angle with respect to the detector, and  $\mu_c$  is the cross-section of the diamond. Taking a single grid into consideration, the distance that the beam traveled  $d_c$  is equal to the grid length  $\Delta w$  divided by  $\sin \varphi_0$ . At this point, we approximate the tilted grid to be up-right, so the absorption of each grid will be a little bigger than in real situation. We set the  $w$  axis along the length of the detector and  $u$  axis along the depth of the detector. Then we set  $y$  and  $z$ -axis pass through the center of the detector.  $Z$ -axis divides the detector into two regions. Since the upper region and the lower region are in phase of  $90^\circ$ , we have to calculate the absorption separately.

For rays from front the top surface, we divide the diamond into layers parallel to the surface x-ray enters and are with thickness of 0.010 mm.

1. For each beamlet, we calculate the absorbed photon flux at each photon energy using the x-ray attenuation data of diamond extracted from XOP database. The absorbed flux spectrum is integrated to obtain the total x-ray power lost by the beamlet in the layer. In this way, we derive the absorbed power as a function of vertical position.
2. The x-ray power absorbed by each detector pixel is calculated by interpolating the function of absorbed power using the  $y$ -coordinates of the pixel center, and scaled according to the volume ratio of the pixel to the volume of the beamlet-layer (beamlet cross section  $\times$  layer depth).
3. The power absorbed by each pixel is then converted into charge density with a simple conversion factor of 13 eV/pair. The time of the x-ray absorption  $t_0=z/c$  is taken as the time of charge-pair creation, where  $z$  is the coordinates of the detector pixel and  $c$  is the speed of light.

Figure 2-4 shows the pixel grid in  $y$ - $z$  space. It confirms that the pixel positions are calculated correctly. Figure 2-5 shows the power absorbed by each pixel plotted against its vertical position. Looking at the pixels on the first layer hit by the incoming x-ray beam, those in the lower half received higher power for two reasons: (1) the x-ray beam is nearly in normal incidence; and (2) the beam center strikes the lower half in this geometry. Referring back to Figure 2-3, we can see the shape of the power distribution follows the pattern for  $y$  from 0 to 0.2 mm. Each line represents each layer of the diamond detector, and the number of grid decreases with the increasing  $y$  value. For the upper region, since the distance that the X-ray traveled through is defined as  $\Delta w / \sin \varphi_0$  and the tilted angle is smaller comparing the lower region, we can notice that the separation between two "lines" is wider than the separation of lower region. For both regions, with the exponentially decreasing beam intensity, the points become more and more dense towards the low energy area.

From Figure 2-4, we can see that the pixel center on the top layer corresponds to the second or third column if viewed from the front surface. Hence in Figure 2-5, the first layer data has an absorbed power curved nearly connects to the third tier for the power in the lower half of the detector. Figure 2-6 shows the power absorbed by each pixel against its layer coordinates. The first column represents pixels on the top layer of the diamond detector.

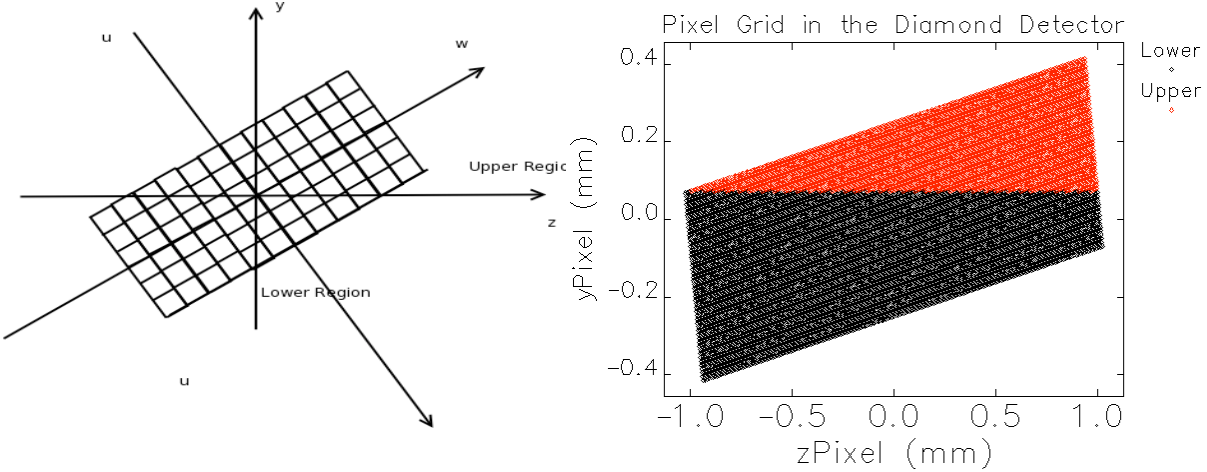


Figure 2-4: Left: Coordinate system used in this simulation. Right: Pixel grid in the diamond detector.

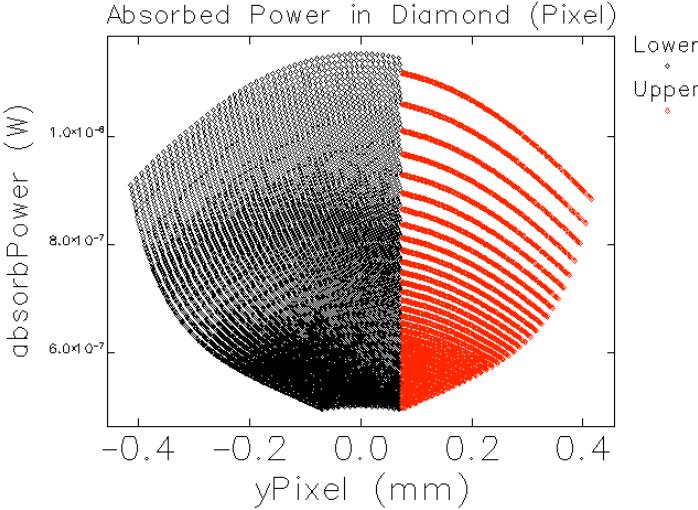


Figure 2-5: The absorbed power in each pixel plotted against its vertical position.

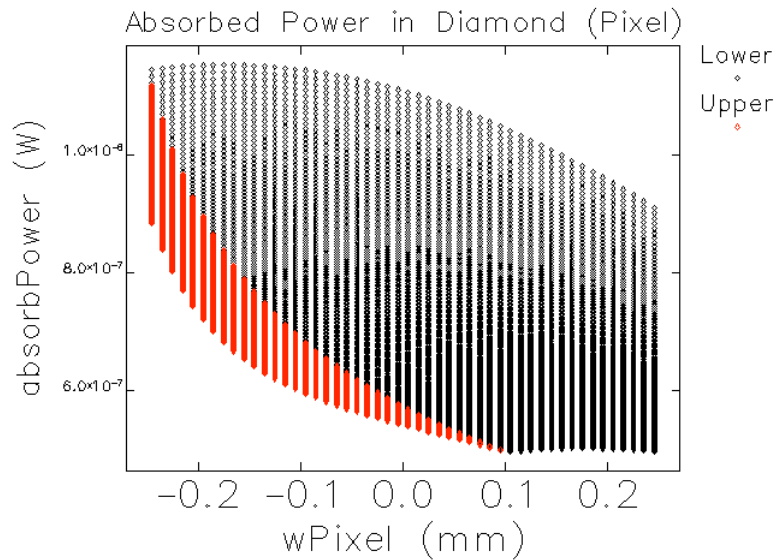


Figure 2-6: The absorbed power in each pixel plotted against its longitudinal position.

By summing up the power absorption of each grid, we found the total absorption by the diamond detector. The total power absorption by diamond is 7.3 mW, which is 7.3% of the beam power after beryllium filter.

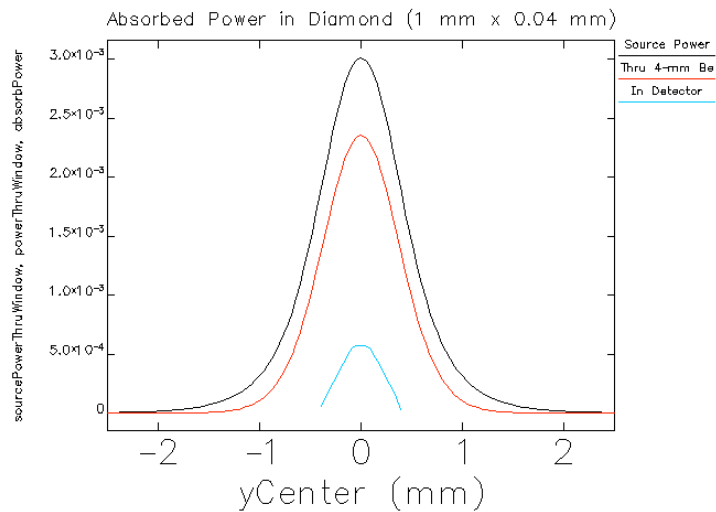


Figure 2-7: The vertical power profiles of the absorbed x-ray beam in the detector (blue), compared with the original source power (black) and the power downstream of the 4-mm beryllium window.

### 2.3 Simulation of charge transfer in the solid ion chamber

To simulate the charge transfer inside the diamond detector, we assume that the transport speed of the charges are

$$v_e = \eta_e \frac{V}{d} \text{ and } v_h = \eta_h \frac{V}{d}, \quad (2.1)$$

where  $\eta_e$  and  $\eta_h$  are mobility of the electrons and holes in diamond, respectively,  $V$  is the applied voltage across the thickness  $d$  of the diamond detector. Table 2-2 lists the parameters used in the simulation. Note that we have neglected effect of charge traps and recombination in the bulk of diamond, and charge injection at the surface of diamond.

Table 2-2: Parameters used for charge transport simulation

Parameter	Value	Units
Average energy per electron-hole pair	13	eV
Electron mobility, $\eta_e$	1800	cm <sup>3</sup> /(Vs)
Hole mobility, $\eta_h$	1200	cm <sup>3</sup> /(Vs)
Saturation charge carrier speed	0.220	mm/ns

The charge transport simulation following a simple procedure:

1. For every time step,  $t$ , we remove any charge that has not been created by then, ( $t_0 > t$ ).
2. We then calculate the position of the remaining electrons and holes in an infinite media,  $w = w_0 + v(t - t_0)$ .
3. Next, we remove all charges outside the finite detector and sum the remaining electron and hole charges. Assuming the charges are traveling at the speed given by Eq. (2.1), we can convert the charges into electron current and hole current, respectively.
4. The current at time  $t$  is obtained by summing the electron and charge current.

Figure 2-8 shows the calculated waveforms for different voltage applied. Due to carrier speed saturation, the waveforms for applied voltages 750V and 1000V are identical. In this simple model, the width of the rising edge is given by the time for the x-ray pulse to traverse the detector, while the applied voltage is approximately proportional to the height of the signal and the width of the pulse, up to the saturation point. 1.

The above discussion only corresponds to one specific time (maximum power) of the incoming beam, of which the power does not keep constant at all time. The power of the incoming beam has a Gaussian distribution. So we select several points on the distribution, then calculated the current for each point and made the summation of current at all time.

Finally, these procedures described earlier are applied many times to generate a database of waveforms with the vertical beam center varying from -6 mm to +6 mm.

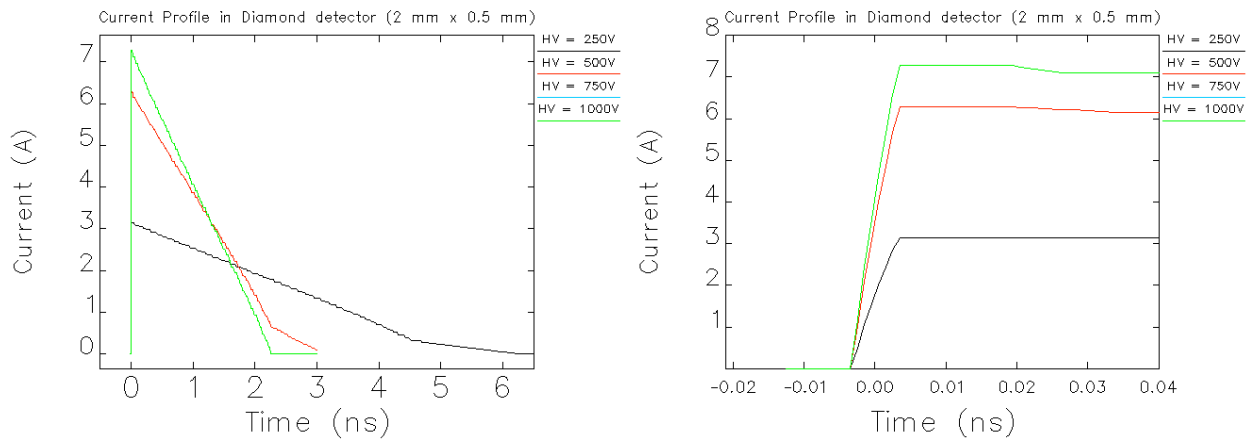


Figure 2-8: The current measured by the detector with respect to time.

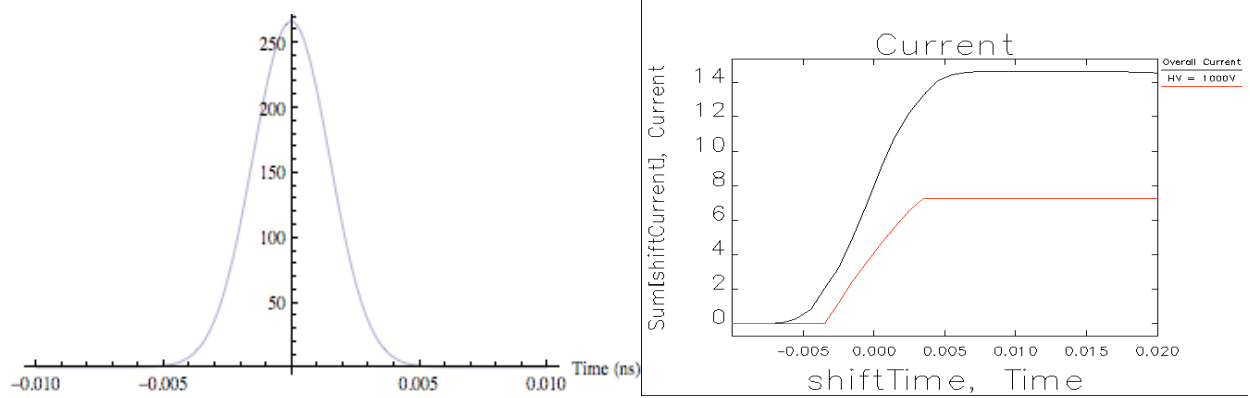


Figure 2-9: Left: power distribution of the beam according to time. Right: total current measured by the detector with respect to time.

The results of current profile are displayed in Figure 2-10. The red line and black line represents two detectors at different position on the copper substrate. The graphs clearly show that there is a phase difference between the two detectors. From the detected phase difference, we can calculate the tilted angle of the x-ray beam according to the positions of the detectors.

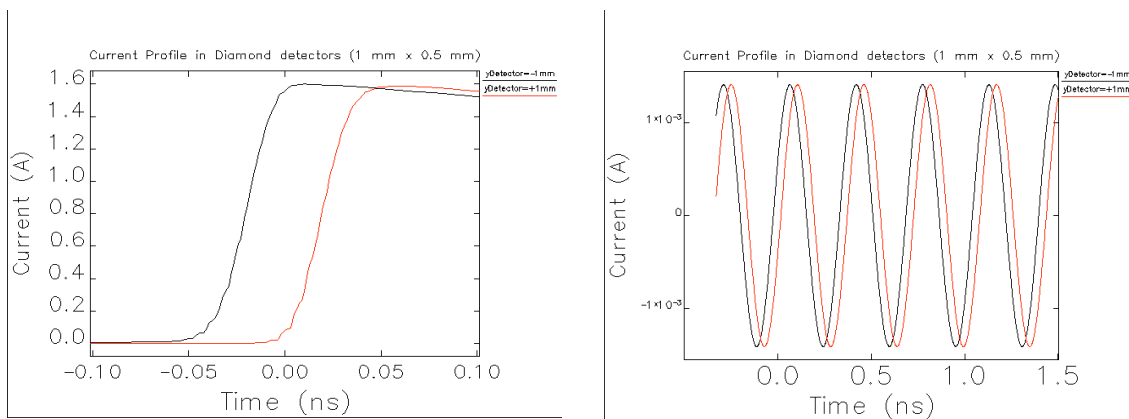


Figure 2-10: waveforms for two different detectors

## 2.4 Simulation of the secondary signal by copper XRF

To be more precise, we have to consider the fluorescence generated by copper, because the diamond detector is able to receive the fluorescence power from the copper substrate as well. The copper substrate measures  $20 \times 2.5 \times 0.5 \text{ mm}^3$ , and the geometry is illustrated in Figure 2-11.

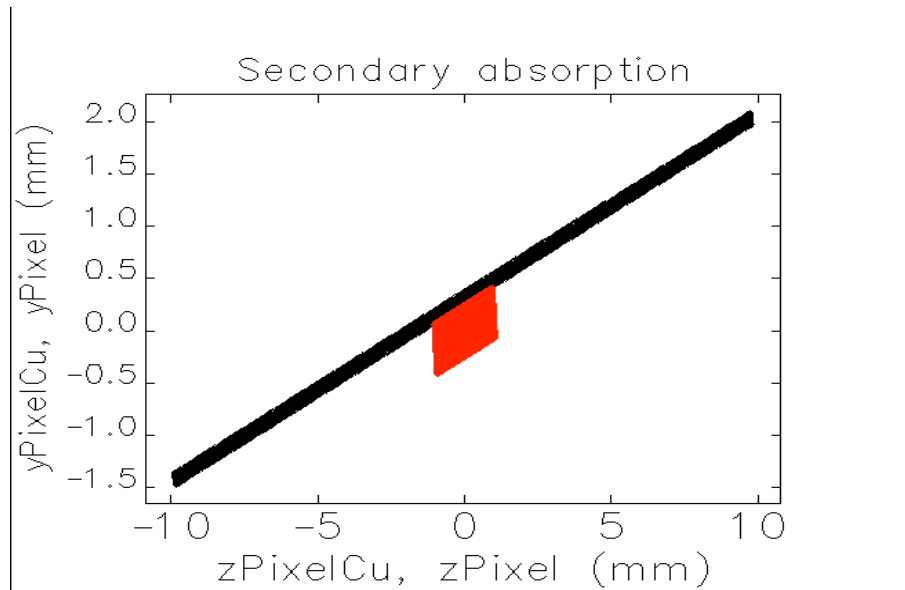


Figure2-11: Geometry for secondary absorption(XRF)

The simulation process for secondary absorption (copper XRF) is as following:

1. The input signal is the resulted beam passing through the two layers of diamond. We filtered the photons with energy less than 9KeV (K-Edge) since they will not be able to cause fluorescence.
2. Using the same procedure as described in the primary absorption, we generated the power absorption of each grid in copper. Then we convert the absorbed power into absorbed photon number. Since fluorescence occurs at two different energy edges ( $k\alpha_1 = 8028\text{eV}$ ,  $k\alpha_2 = 8048\text{eV}$ ) for copper, we approximate the emitting photon energy to be 8040eV.
3. We then calculate the path length of the x-ray fluorescence traveled through each media (copper or diamond) because of the different attenuation. The attenuation for copper is 464.565 1/mm, and the attenuation for diamond is 15.921 1/mm. Then we have the the total transmitted number of photons at a certain layer (sphere).
4. Since copper's fluorescence radiates isotropically in  $4\pi$  solid angle, we have to work out the proportion of the area of each grid to the sphere's surface area. Then after multiplying the transmitted photon numbers at a spherical layer with the area factor, we have the total number of photons absorbed into one diamond grid.

Then we calculated the total absorbed power due to copper fluorescence and the result is 0.14mW, which is around 2% of the primary absorption.

## **5. Summary and discussion**

From the calculated power absorption of diamond tilt monitor, our proposed model can generate a database of waveforms for detectors at different position. Using the phase differences from the waveform database, we are able to calculate the x-ray's tilted angle. However, since the realistic monitor has not been built yet, we cannot compare the results of our simulation from the experimental data.

During the simulation process, the primary or direct absorption of x-ray beam contributes most of the signal to the detector. Though we thought the fluorescence generated by copper is able to affect the final signals, actually it only has very small influence. We made several approximations during the simulation, especially in calculating the attenuation of x-ray beam in different materials. However, the result, from the perspective of power absorption and waveforms, is sound and reasonable, and we believe the simulation of the diamond tilt monitor is successful.

## [References]

- [1] Advanced Photon Source Upgrade Conceptual Design Report, November 2010.
- [2] Bingxin Yang and Robert Lill, Initial test of diamond detectors, APS-ASD-DIAG Tech Note, DIAG-TN-2010-011, July, 2010.
- [3] M. Sanchez del Rio and R. J. Dejus, Status of XOP: an x-ray optics software toolkit, SPIE Proceedings Vol. 5536 (2004) pp.171-174.
- [4] M. Borland, A self-describing file protocol for simulation integration and shared postprocessors, Proc. of the 1995 Particle Accelerator Conference, May 1995, Dallas.  
([http://www.aps.anl.gov/Accelerator\\_Systems\\_Division/Operations\\_Analysis/manuals/SDDStoolkit/SDDStoolkit.html](http://www.aps.anl.gov/Accelerator_Systems_Division/Operations_Analysis/manuals/SDDStoolkit/SDDStoolkit.html))
- [5] Hairong Shang adapted Roger Dejus' wiggler source program ws from FORTRAN to c and included it as part of the sdds tools, private communication.
- [6] D. R. Kania, m. i. Landstrass, M. A. Plano, L. S. Pan, and S. Han, Diamond radiation detectors, Diamond and Related Materials 2 (1993) pp. 1012-1019.
  
- [5] N. Sereno, M. Borland, R. Lill, Automated correction of phase errors in the Advanced Photon Source linac, Phys. Rev. ST Accel. Beams 11, 072801 (2008)  
<http://prst-ab.aps.org/abstract/PRSTAB/v11/i7/e072801>
  
- [4] D. R. Kania, L. S. Pan, P. Bell, O. L. Landen, H. Kornblum, and P. Pianetta, Absolute x-ray power measurements with subnanosecond time resolution using type IIa diamond photoconductors, J. Appl. Phys. 68 (124) 1990.